Electronic Supplementary Material (ESI) for Dalton Transactions.

Supporting Information

Construction of Copper Chains with New Fluorescent Guanidino-Functionalized Naphthyridine Ligands

Christoph Krämer, Simone Leingang, Olaf Hübner, Elisabeth Kaifer, Hubert Wadepohl, Hans-Jörg Himmel*

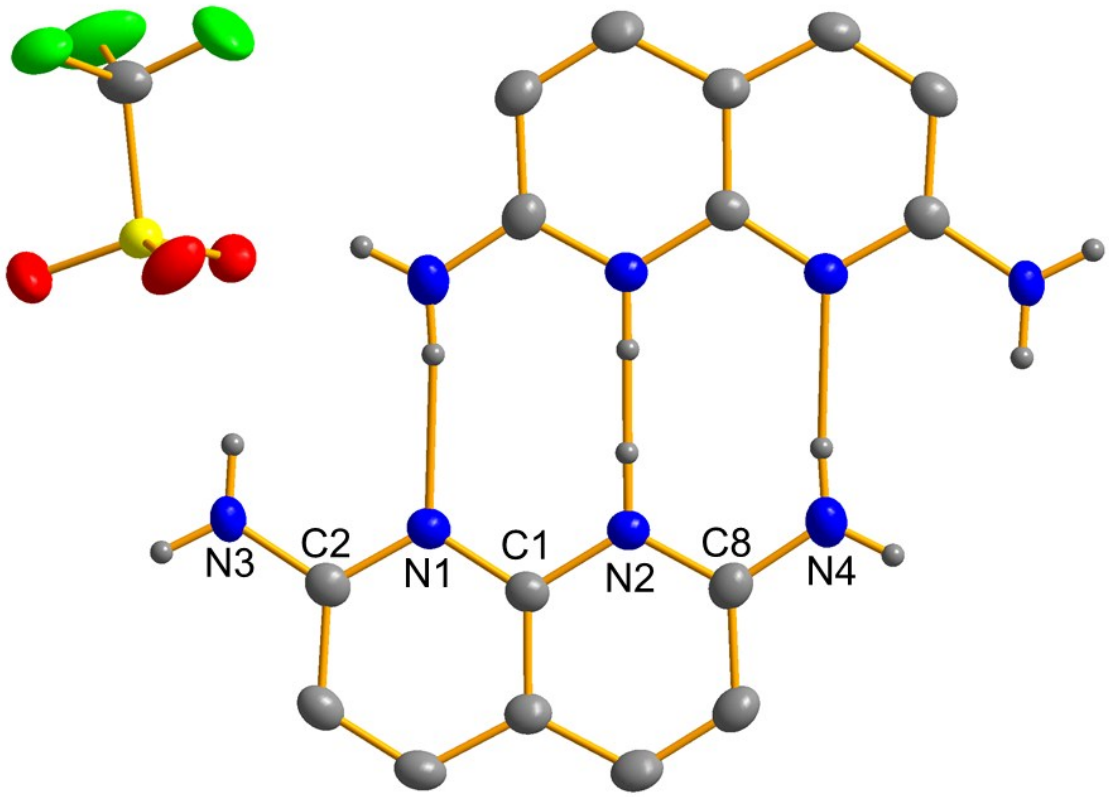

Fig. S1 Hydrogen-bonded dimer of the protonated amino precursor to the guanidino ligands. A double-potential minimum exists with the proton on one or the other molecule. Hydrogen atoms attached to carbon omitted for clarity. Vibrational ellipsoids drawn at the 50% probability level. Selected bond distances (in Å): N1-C1 1.355(2), N1-C2 1.338(2), N2-C1 1.373(2), N2-C8 1.349(2), N3-C2 1.383(2), N4-C8 1.331(2), N1···N4' 2.883(1), N2···N2' 2.995(1).

UV/Vis

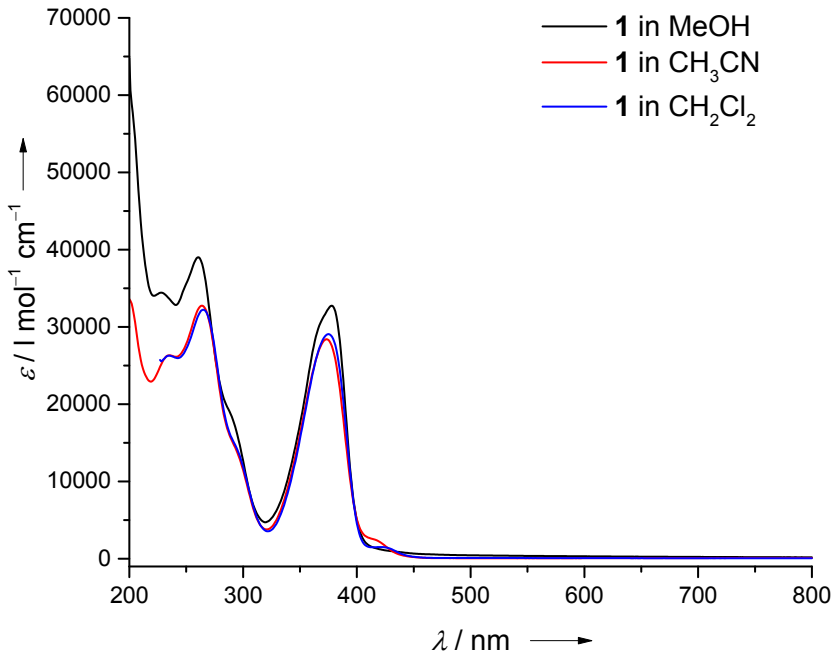

Fig. S2 Comparison of the UV/Vis spectrum of **1** in different solvents (c = $2.0 \cdot 10^{-5}$ mol l^{-1}).

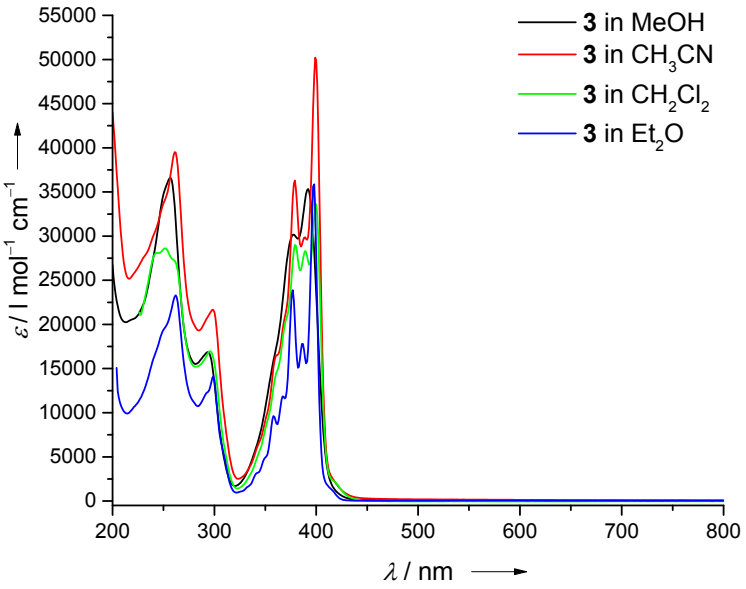

Fig. S3 Comparison of the UV/Vis spectrum of **3** in different solvents (c = $2.0 \cdot 10^{-5}$ mol l^{-1}).

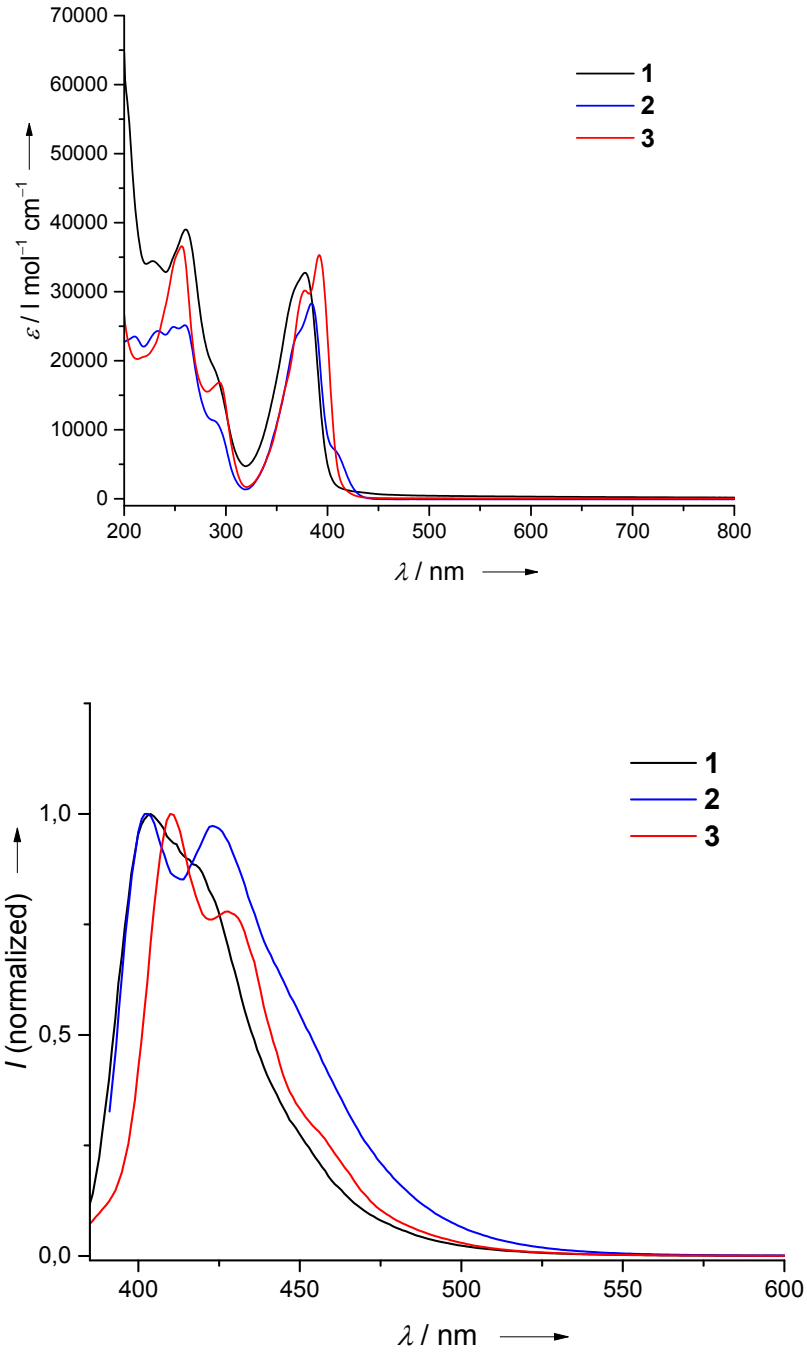

Fig. S4 Top: UV/Vis spectra of **1**, **2** and **3** in CH_3OH ($c = 2.0 \cdot 10^{-5}$ mol l^{-1}). Bottom: Normalized emission spectra of **1**, **2** and **3** in CH_3OH ($c = 2.0 \cdot 10^{-5}$ mol l^{-1}).

CV measurements

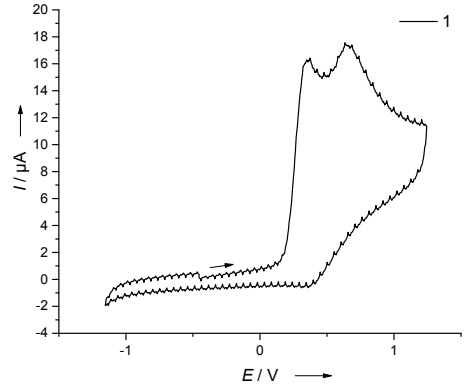

Fig. S5 CV of **1** (potential vs Fc/Fc^+, CH_2Cl_2 solution, with [*n*-Bu_4N][PF_6] as supporting electrolyte, scan speed of 100 mV s^{-1}.

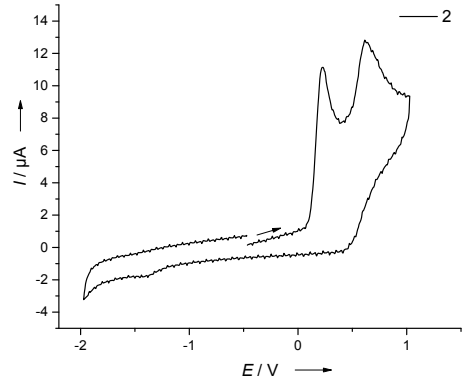

Fig. S6 CV of **2** (potential vs Fc/Fc^+, CH_2Cl_2 solution, with [*n*-Bu_4N][PF_6] as supporting electrolyte, scan speed of 100 mV s^{-1}.

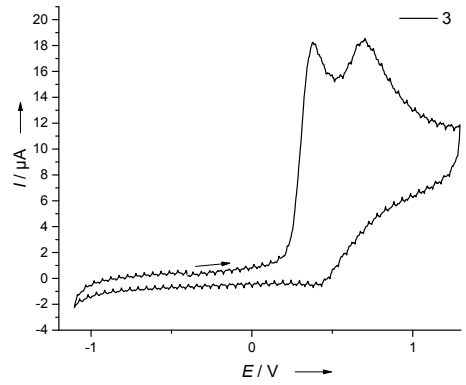

Fig. S7 CV of **3** (potential vs Fc/Fc^+, CH_2Cl_2 solution, with [*n*-Bu_4N][PF_6] as supporting electrolyte, scan speed of 100 mV s^{-1}.

NMR

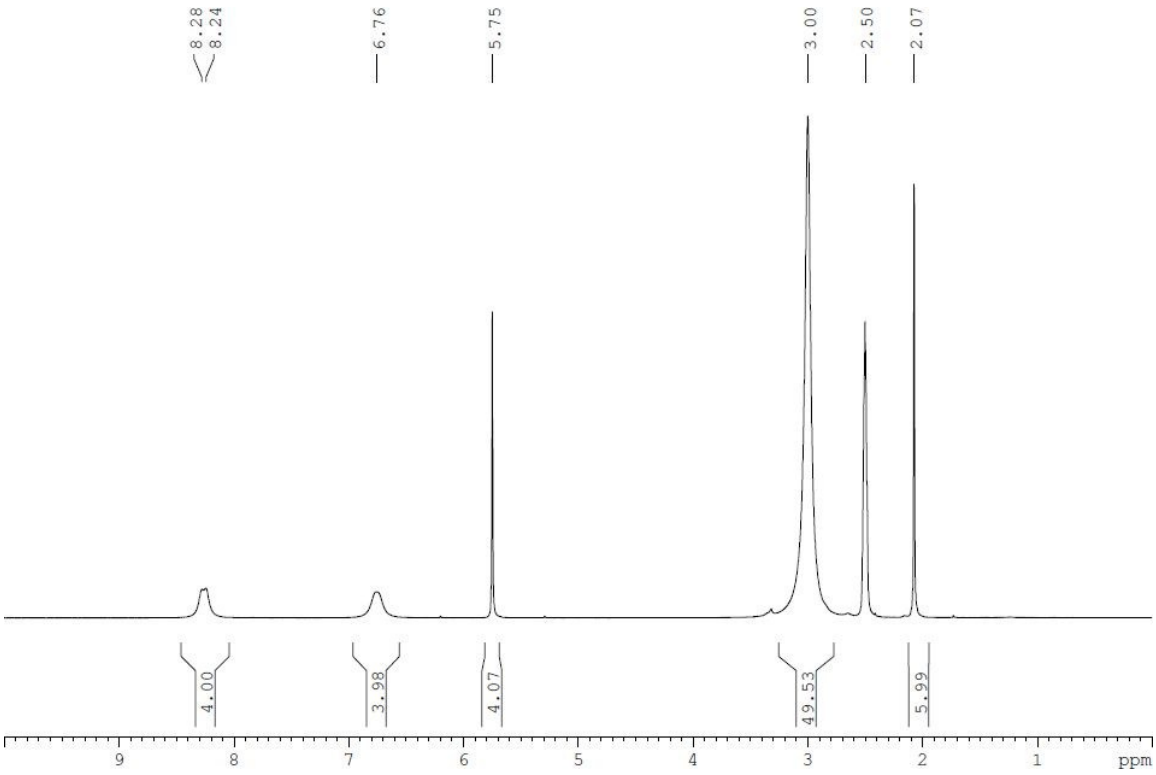

Fig. S8 ^1H NMR (199.87 MHz, 298.0 K) spectrum of $[Cu_4(\mathbf{1})_2](BF_4)_4 \cdot 2CH_3CN$ in *d6*-DMSO, showing the presence of uncoordinated CH_3CN molecules (signal at δ = 2.07 ppm).

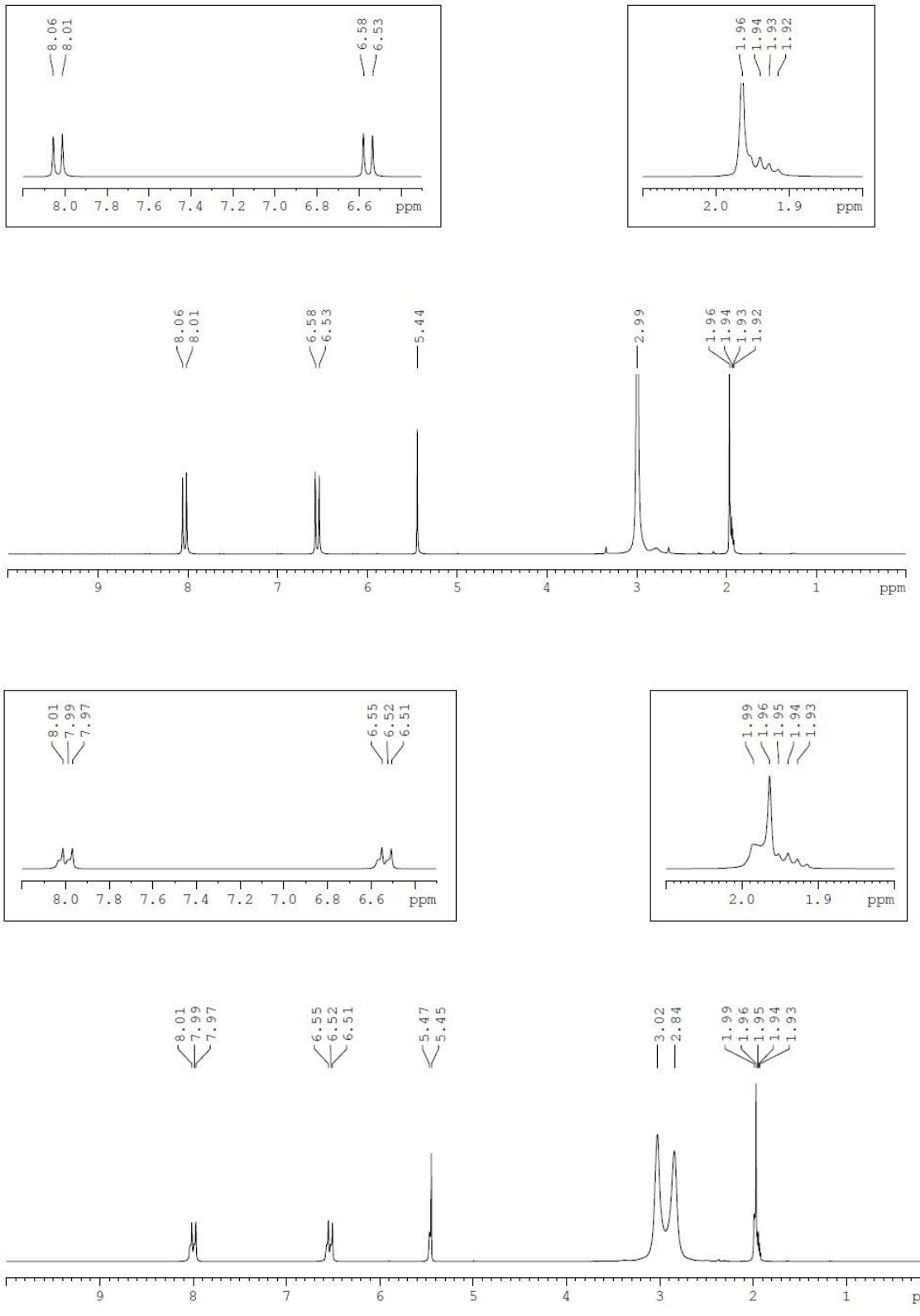

Fig. S9 ^{1}H NMR (199.87 MHz) spectra of $[Cu_4(\mathbf{1})_2](BF_4)_4 \cdot 2CH_3CN$ in CD_3CN at 25 °C (top) and −35 °C (bottom), indicating coordination of CH_3CN molecules at low temperature.

Experimental details

I) Substitution of CH_3CN in $[Cu_4(\mathbf{1})_2](BF_4)_4 \cdot 2CH_3CN$

a) 7.30 mg (0.06 mmol, 4.0 eq) 4-(dimethylamino)pyridine was added to a solution of 20.0 mg (0.02 mmol, 1.0 eq) $[Cu_4(\mathbf{1})_2](BF_4)_4 \cdot 2CH_3CN$ in 4 ml CH_3CN. The solution was stirred for 3 d at room temperature. Then, the solvent was removed in vacuo and a brown solid was obtained. No reaction could be observed by ^{1}H NMR and MS.

b) 3.72 mg (0.03, 2.0 eq) 2-nitropyridine was added to a solution of 20.0 mg (0.02 mmol, 1.0 eq) $[Cu_4(\mathbf{1})_2](BF_4)_4 \cdot 2CH_3CN$ in 4 ml CH_3CN. After the solution was stirred for 1h at room temperature, the solvent was removed. As ^{1}H NMR showed that no reaction took place, the solid was redissolved in CH_3CN and the solution was heated at reflux for 3 h. Analytical data showed that no reaction occurred.

c) 34.5 mg (0.02 mmol, 1.0 eq) $[Cu_4(\mathbf{1})_2](BF_4)_4 \cdot 2CH_3CN$ was dissolved in 3 ml benzonitrile. The solution was stirred for 3 d at room temperature. Then, the excess of benzonitrile was removed under reduced pressure. The resulting yellow solid was washed with hexane (3x5 ml) and redissolved in 10 ml CH_2Cl_2, insoluble solid was filtered off. The insoluble solid was identified as $[Cu_4(\mathbf{1})_2](BF_4)_4 \cdot 2CH_3CN$ by ^{1}H-NMR. X-Ray structure analysis of the crystals obtained from CH_2Cl_2 solution revealed a mixture of $[Cu_4(\mathbf{1})_2(CH_2Cl_2)_2](BF_4)_4$, $[Cu_4(\mathbf{1})_2](BF_4)_4$ and $[Cu_4(\mathbf{1})_2(CuCl_2)_2](BF_4)_2$ (see Fig. S11). Crystal data for $[Cu_4(\mathbf{1})_2(CH_2Cl_2)_2](BF_4)_4$, $[Cu_4(\mathbf{1})_2](BF_4)_4$, $[Cu_4(\mathbf{1})_2(CuCl_2)_2](BF_4)_2$, $C_{110}H_{172}B_{10}Cl_8Cu_{14}F_{40}N_{48} \cdot 6CH_2Cl_2$: Mr = 4717.76, 0.10 x 0.08 x 0.06 mm^3, triclinic, space group $P\bar{1}$, a = 12.7803(3), b = 15.1583(4), c = 23.8968(6) Å, α = 100.103(2)°, β = 100.290(2)°, γ = 91.496(2)°, V = 4476.5(2) Å^3, Z = 1, d_{calc} = 1.750 Mg·m^{-3}, Mo K_α radiation (λ = 0.71073 Å), μ = 2.024 mm^{-1}, T = 120(1) K, θ-range 3.2 to 26.4°. Reflections measd. 165973, indep. 18252 [R_{int} = 0.0833], obs. 14220. Final R indices [$I > 2\sigma(I)$]: $R(F)$ = 0.0486, $wR(F^2)$ = 0.1096, $GooF$ = 1.021.

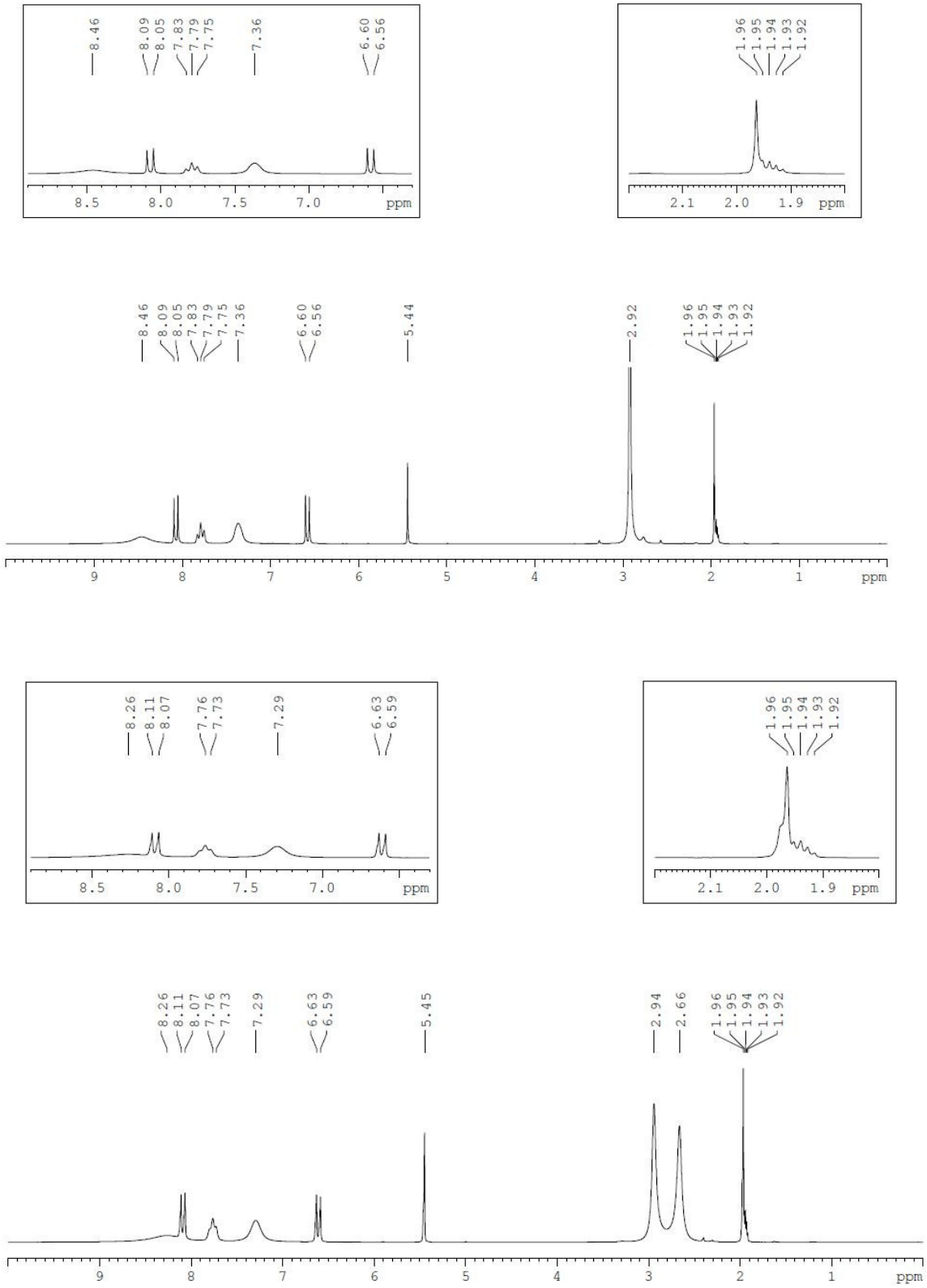

Fig. S10 ^{1}H NMR (199.87 MHz) spectra of $[Cu_4(\mathbf{1})_2](BF_4)_4 \cdot 2CH_3CN$ in the presence of 2 equivalents pyridine in CD_3CN at 25 °C (top) and –35 °C (bottom).

a)

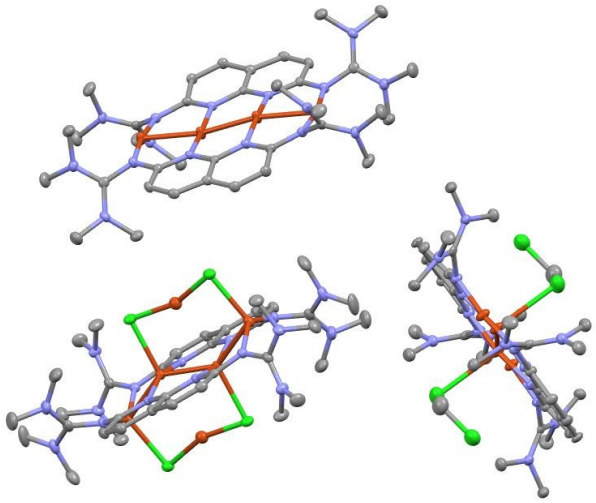

b)

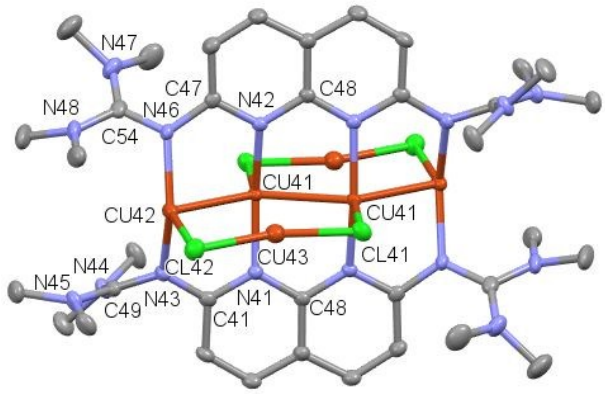

Fig. S11 Molecular structure of $[Cu_4(\mathbf{1})_2(CuCl)_2](BF_4)_2$, $[Cu_4(\mathbf{1})_2](BF_4)_4$ and $[Cu_4(\mathbf{1})_2(CH_2Cl_2)_2](BF_4)_4$. BF_4^- anions, solvent molecules and hydrogen atoms attached to carbon omitted for clarity. Vibrational ellipsoids drawn at the 50% probability level. Selected bond distances (in Å) and angles (in °):

a) View of the unit cell containing the three complexes $[Cu_4(\mathbf{1})_2(CuCl_2)_2]^{2+}$, $[Cu_4(\mathbf{1})_2]^{4+}$ and $[Cu_4(\mathbf{1})_2(CH_2Cl_2)_2]^{4+}$.

b) Structure of $[Cu_4(\mathbf{1})_2(CuCl_2)_2](BF_4)_2$: Cu41···Cu41‘ 2.4520(9), Cu41···Cu42 2.4855(7), Cu41···Cu43 2.9358(7), Cu41-Cl41’ 2.4732(11), Cu42-Cl42 2.4057(11), Cu43-Cl41 2.1301(12), Cu43-Cl42 2.1316(12), Cu41-N41 1.955(3), Cu41-N42 1.958(3), Cu42-N43 1.949(3), Cu42-N46 1.949(3), N41-C41 1.350(5), N41-C48 1.369(5), N42-C47 1.346(5), N42-C48‘ 1.369(5), N43-C41 1.363(5), N43-C49 1.369(5), N44-C49 1.337(5), N45-C49 1.335(5), N46-C47 1.373(5), N46-C54 1.341(5), N47-C54 1.342(6), N48-C54 1.355(6), Cu41‘···Cu41···Cu42 139.44(3), Cu43-Cl41-Cu41‘ 87.58(4), Cu43-Cl42-Cu42 83.51(4), Cl41-Cu43-Cl42 161.04(5), N41-Cu41-N42 161.42(13), N46-Cu42-N43 140.25(14).

c)

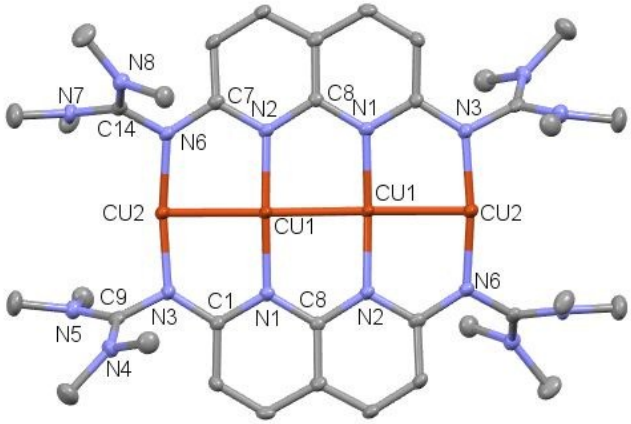

d)

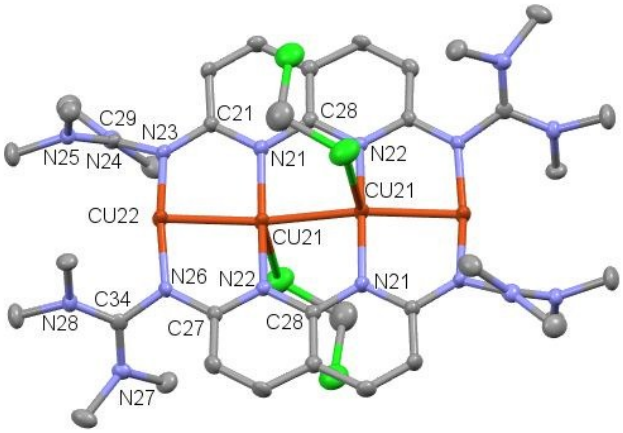

c) Structure of $[Cu_4(\mathbf{1})_2](BF_4)_4$: Cu1···Cu1‘ 2.4162(9), Cu1···Cu2 2.4255(7), Cu1-N1 1.921(3), Cu1-N2 1.917(3), Cu2-N3 1.869(3), Cu2-N6 1.866(3), N1-C1 1.351(5), N1-C8 1.375(5), N2-C7 1.355(5), N2-C8 1.372(5), N3-C1 1.368(5), N3-C9 1.377(5), N4-C9 1.326(5), N5-C9 1.341(5), N6-C7 1.374(5), N6-C14 1.367(5), N7-C14 1.340(5), N8-C14 1.331(5), Cu1‘···Cu1···Cu2 168.69(4), N1‘-Cu1-N2 173.44(14), N6-Cu2-N3‘ 170.52(14).

d) Structure of $[Cu_4(\mathbf{1})_2(CH_2Cl_2)_2](BF_4)_4$: Cu21···Cu21‘ 2.4087(10), Cu21···Cu22 2.4187(7), Cu21-N21‘ 1.937(3), Cu21-N22 1.931(3), Cu22-N23‘ 1.867(3), Cu22-N26 1.868(3), N21-C21‘ 1.356 (5), N21-C28 1.372(5), N22-C27 1.350(5), N22-C28 1.376(5), N23-C21 1.363(5), N23-C29 1.373(5), N24-C29 1.330(5), N25-C29 1.333(5), N26-C27 1.367(5), N26-C34 1.370(5), N27-C34 1.333(5), N28-C34 1.334(5), Cu21‘···Cu21···Cu22 165.13(4), N21‘-Cu21-N22 171.79(15), N26-Cu22-N23‘ 169.61(14).

Experimental details

II) Reaction of $[Cu_4(\mathbf{1})_2](BF_4)_4 \cdot 2CH_3CN$ with bis(triphenylphosphoranylidene)ammonium chloride (PPNCl)

23.6 mg (0.02 mmol, 1.0 eq) of $[Cu_4(\mathbf{1})_2](BF_4)_4 \cdot 2CH_3CN$ and 19.4 mg of PPNCl were dissolved in 5 ml CH_3CN. The solution was stirred for 2 h at room temperature. No reaction was observed in the ^1H NMR spectrum (see Fig. S14) and with ESI^+-MS.

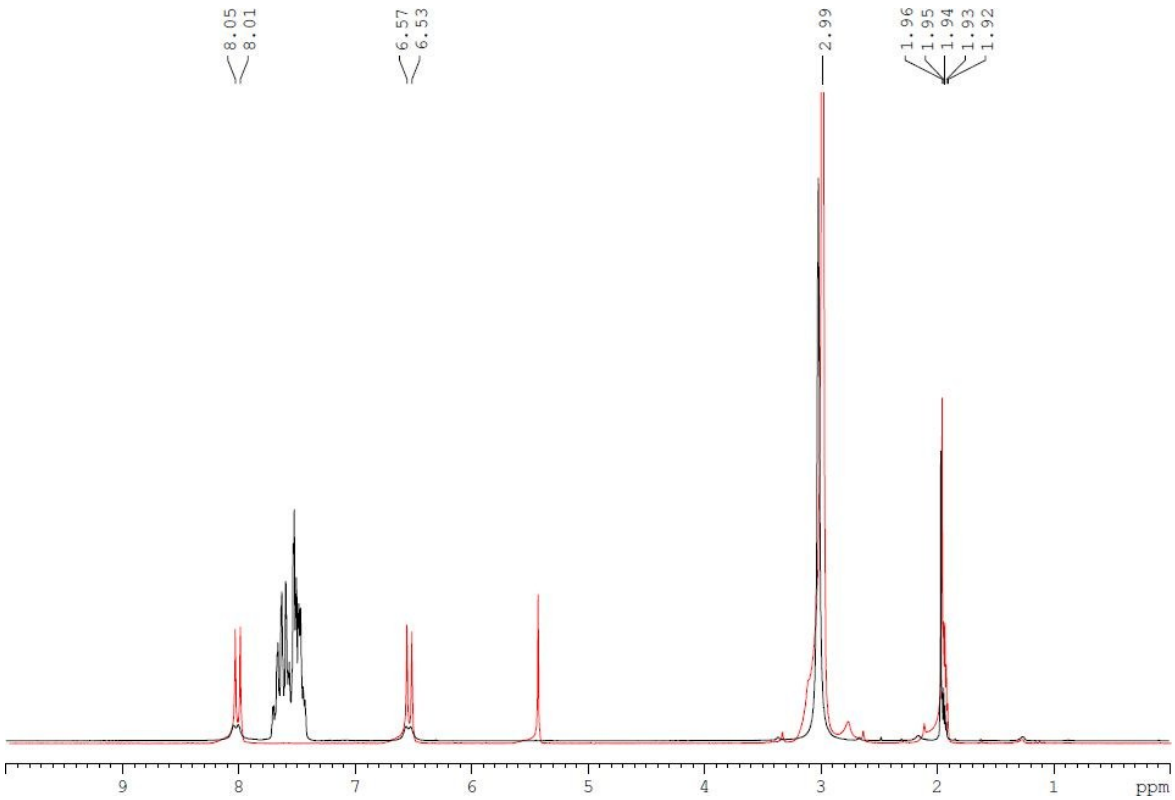

Fig. S12 ^1H NMR (199.87 MHz, 295.0 K, CD_3CN) spectra of $[Cu_4(\mathbf{1})_2](BF_4)_4 \cdot 2CH_3CN$ before (red) and after (black) the addition of PPNCl.

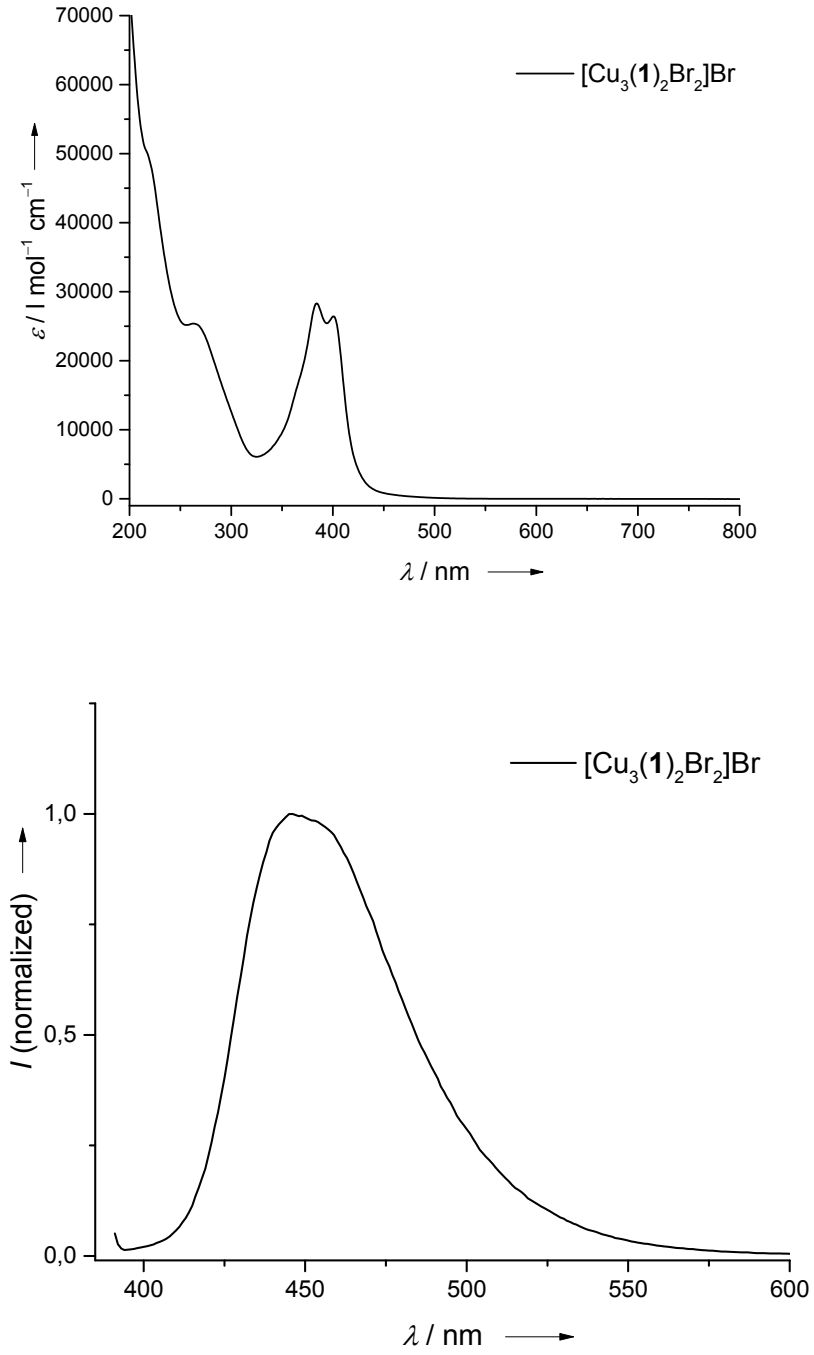

Fig. S13 Top: UV/Vis spectra of $[Cu_3(\mathbf{1})_2Br_2]Br$ in CH_3CN ($c = 1.0 \cdot 10^{-5}$ mol l^{-1}). Bottom: Normalized emission spectra of $[Cu_3(\mathbf{1})_2Br_2]Br$ in CH_3CN ($c = 1.0 \cdot 10^{-5}$ mol l^{-1}).

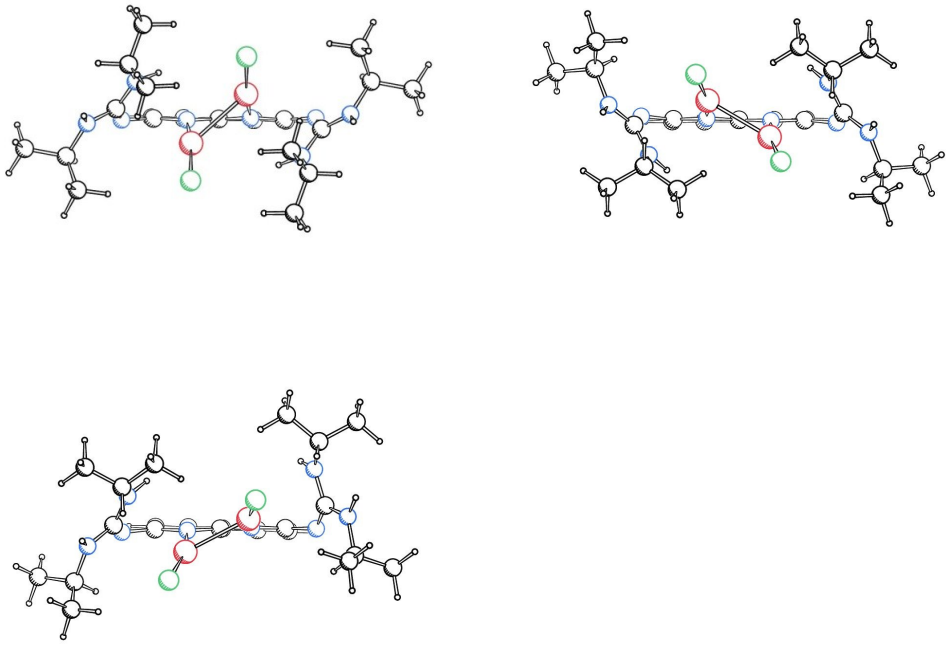

Fig. S14 Visualization of calculated minimum structures of [(CuCl)$_2$**3**] (B3LYP/SV(P)).

Table S1 Comparison of experimental and calculated bond distances (in Å) and angles (in °) for [Cu$_4$(**1**)$_2$]$^{4+}$ and [Cu$_4$(**1**)$_2$(CH$_3$CN)$_2$]$^{4+}$ (B3LYP/SV(P).

	[Cu$_4$(**1**)$_2$]$^{4+}$		[Cu$_4$(**1**)$_2$(CH$_3$CN)$_2$]$^{4+}$	
	exp.	calc.	exp.	calc.
$M_{terminal}\cdots M_{central}$	2.426	2.449	2.486	2.557
$M_{central}\cdots M_{central}$	2.416	2.426	2.491	2.592
$M_{central}$–N	1.917/1.921	1.972	2.000	2.084
$M_{terminal}$–N	1.866/1.869	1.927	1.865	1.919
N=C	1.367/1.377	1.386	1.374/1.376	1.376
M-M-M	168.69	170.70	140.65	128.22

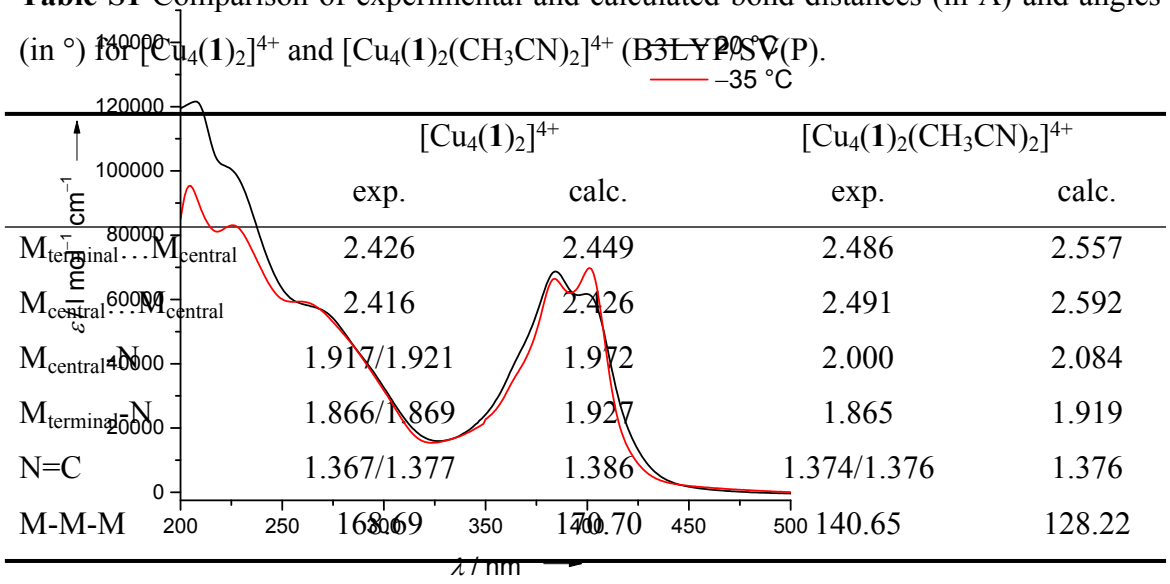

Fig. S15 UV/Vis spectra of [Cu$_4$(**1**)$_2$](BF$_4$)$_4$ in CH$_3$CN solution at 20 °C and –35 °C.

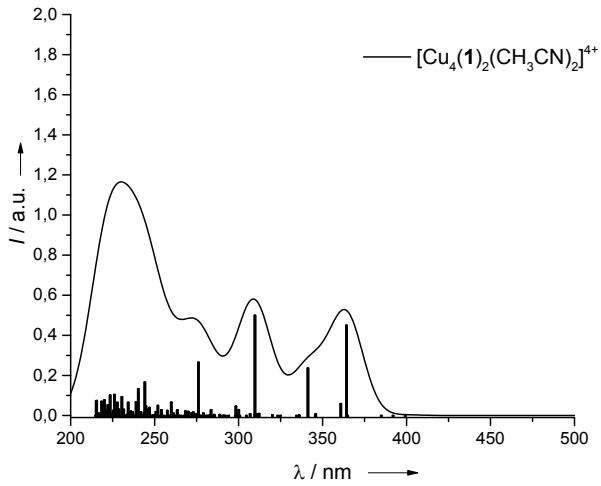

Fig. S16 Theoretical UV/Vis spectrum from TD-DFT calculations (B3LYP/def2-SV(P)) for $[Cu_4(\mathbf{1})_2(CH_3CN)_2]^{4+}$. The spectrum was simulated with Gaussian functions of a half-width of 20 nm.

Experimental details

III) Catalysis

1-benzyl-4-phenyl-1H-1,2,3-triazole

5.9 mg (4.2 µmol, 1.0 mol%) $[Cu_4(\mathbf{1})_2](BF_4)_4 \cdot 2CH_3CN$ were dissolved in 0.5 ml *d6*-DMSO. 50 µl (0.46 mmol, 1.04 eq) phenylacetylene and 55 µl (0.44 mmol, 1.0 eq) benzyl azide were added. The solution was stirred overnight. ^{1}H NMR showed complete reaction. The NMR spectrum is shown in Fig. S17. ^{1}H NMR (199.87 MHz, *d6*-DMSO, 295.0 K): δ = 5.61 (s, 2 H, -C*H*$_2$-), 7.24-7.43 (m, 8 H, C*H*$_{arom.}$), 7.82 (d, J = 6.86 Hz, 2 H, C*H*$_{arom.}$) ppm, 8.60 (s, 1H, -C*H*-).

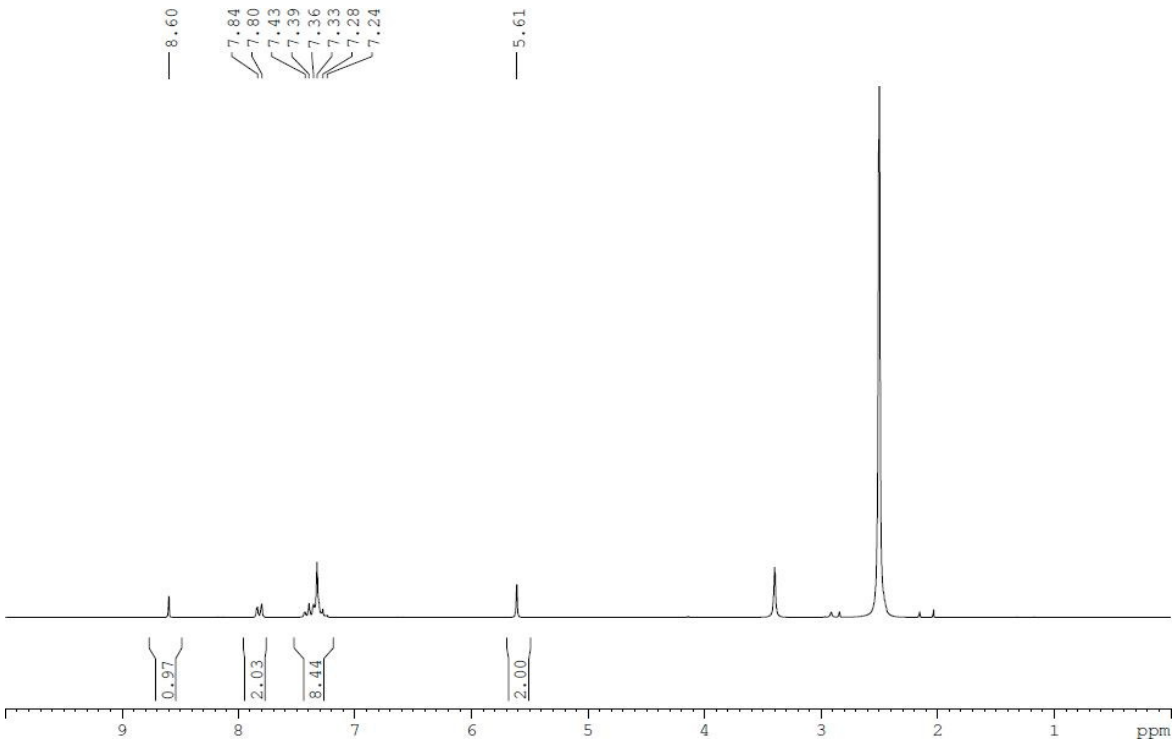

Fig. S17 ^{1}H NMR (199.87 MHz, 295.0 K) spectrum of 1-benzyl-4-phenyl-1*H*-1,2,3-triazole in d_6-DMSO.

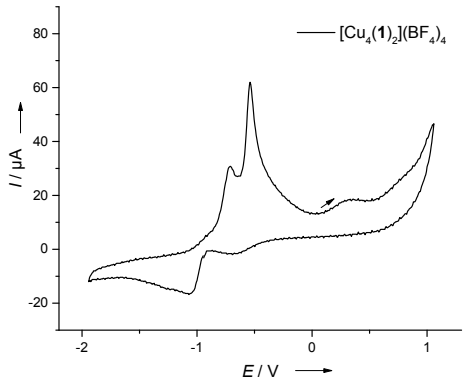

Fig. S18 CV of $[Cu_4(\mathbf{1})_2](BF_4)_4$ (potential vs Fc/Fc^+, CH_3CN solution, with $[n\text{-}Bu_4N][PF_6]$ as supporting electrolyte, scan speed of 500 mV s^{-1}.

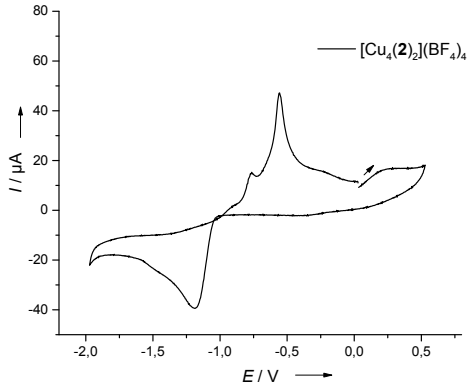

Fig. S19 CV of $[Cu_4(\mathbf{2})_2](BF_4)_4$ (potential vs Fc/Fc^+, CH_3CN solution, with $[n\text{-}Bu_4N][PF_6]$ as supporting electrolyte, scan speed of 500 mV s^{-1}.

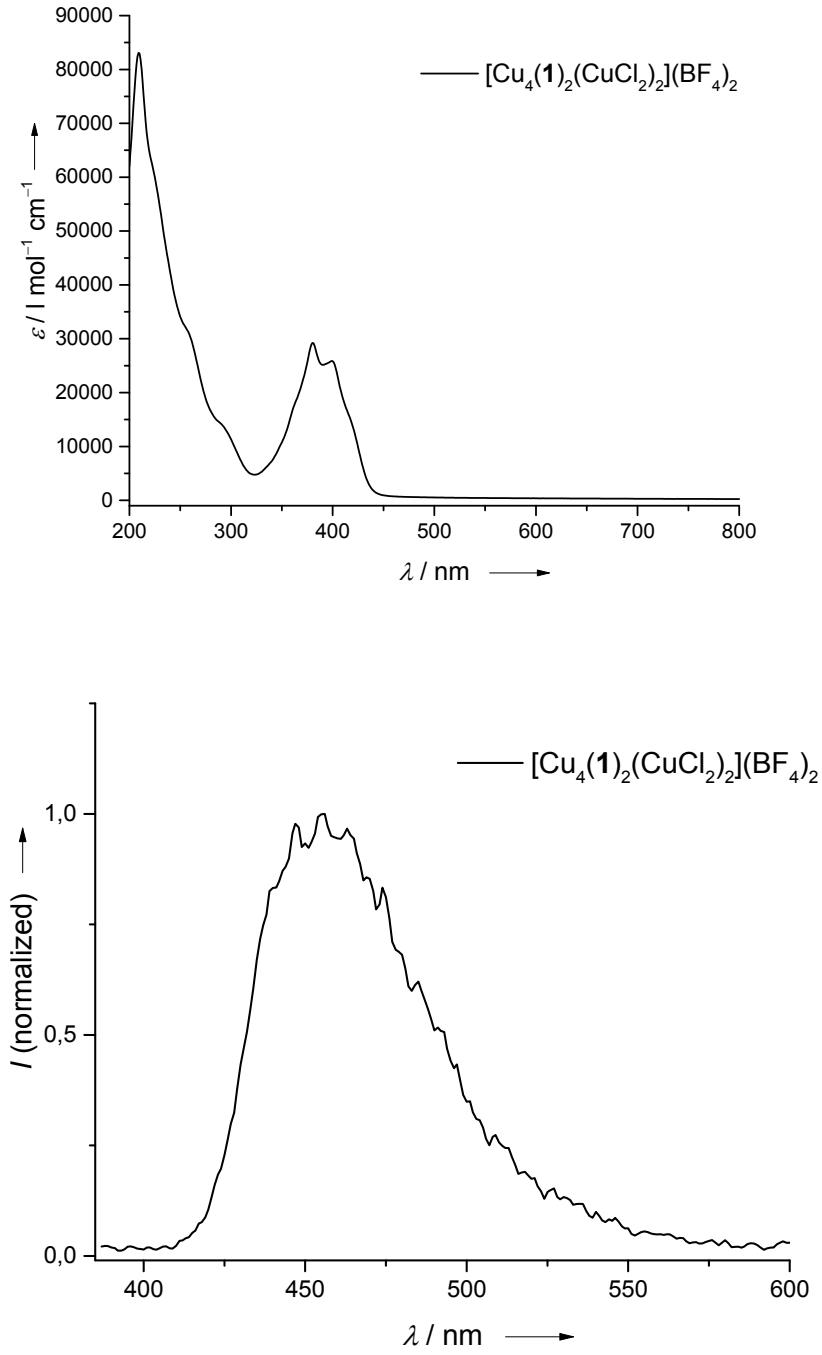

Fig. S20 Top: UV/Vis spectra of $[Cu_4(\mathbf{1})_2(CuCl_2)_2](BF_4)_2$ in CH_3CN (c = $1.2 \cdot 10^{-5}$ mol l^{-1}). Bottom: Normalized emission spectra of $[Cu_4(\mathbf{1})_2(CuCl_2)_2](BF_4)_2$ in CH_3CN (c = $1.2 \cdot 10^{-5}$ mol l^{-1}).

Experimental details

IV) Oxidation of $[Cu_4(\mathbf{1})_2](BF_4)_4 \cdot 2CH_3CN$

a) 22.2 mg (0.02 mmol, 1.0 eq) $[Cu_4(\mathbf{1})_2](BF_4)_4 \cdot 2CH_3CN$ was dissolved in 4 ml CH_3CN. 9.28 mg (0.04 mmol, 2.0 eq) ferrocenium tetrafluoroborate were added. The solution was stirred for 4 h at room temperature. Then, the solution was removed under reduced pressure. No reaction observed. The reaction was repeated heating the solution at reflux for 3.5 h. Also this time no reaction took place.

b) 15.3 mg (0.01 mmol, 1.0 eq) $[Cu_4(\mathbf{1})_2](BF_4)_4 \cdot 2CH_3CN$ was dissolved in 3 ml CH_3CN. 2.70 mg (0.02 mmol, 2.0 eq) benzoquinone were added. The solution was first stirred for 1 h at room temperature, then 1.5 h at 50 °C and finally at 80 °C overnight. Afterwards, the solvent was removed in vacuo receiving a brownish solid. No reaction observed in ^1H NMR spectrum.

c) 17.9 mg (0.01 mmol, 1.0 eq) $[Cu_4(\mathbf{1})_2](BF_4)_4 \cdot 2CH_3CN$ was dissolved in 5 ml CH_3CN and cooled down to -35 °C. Then a solution of 1.5 mg (0.01 mmol, 1.0 eq) $NOBF_4$ in 2 ml CH_3CN was added dropwise. Thereby the solution turned colorless. After the addition was completed, the solution was stirred for 1 h at -35 °C and the solution turned slightly green. Finally, the solid was removed in vacuo. Analysis showed decomposition of the compound.

d) 20.0 mg (0.01 mmol, 1.0 eq) $[Cu_4(\mathbf{1})_2](BF_4)_4 \cdot 2CH_3CN$ were dissolved in 4.5 ml CH_3CN. A solution of 5.6 mg (0.03 mmol, 2.0 eq) solved in 2.5 ml CH_3CN were added dropwise. The solution was stirred for 30 min at room temperature. After 2 min of stirring, the color of the solution turned from yellow to colorless. After 30 min, the solvent was removed under reduced pressure and a slightly yellow solid was obtained. NMR analysis showed decomposition of the compound.

V) Reaction of KCl/CuCl with $[Cu_4(\mathbf{1})_2](BF_4)_4 \cdot 2CH_3CN$

15.2 mg (0.01 mmol, 1.0 eq) $[Cu_4(\mathbf{1})_2](BF_4)_4 \cdot 2CH_3CN$, 1.70 mg (0.02 mmol, 2.0 eq) KCl and 2.20 mg (0.02 mmol, 2.0 eq) CuCl were suspended in 4 ml CH_3CN. The reaction mixture was stirred overnight at 75 °C. After cooling to room temperature, the solvent was removed in vacuo. The obtained yellow solid was redissolved in CH_2Cl_2 in order to grow crystals,

insoluble solid was filtered off. However, no crystals were received and further analytical data showed that no reaction has occurred.

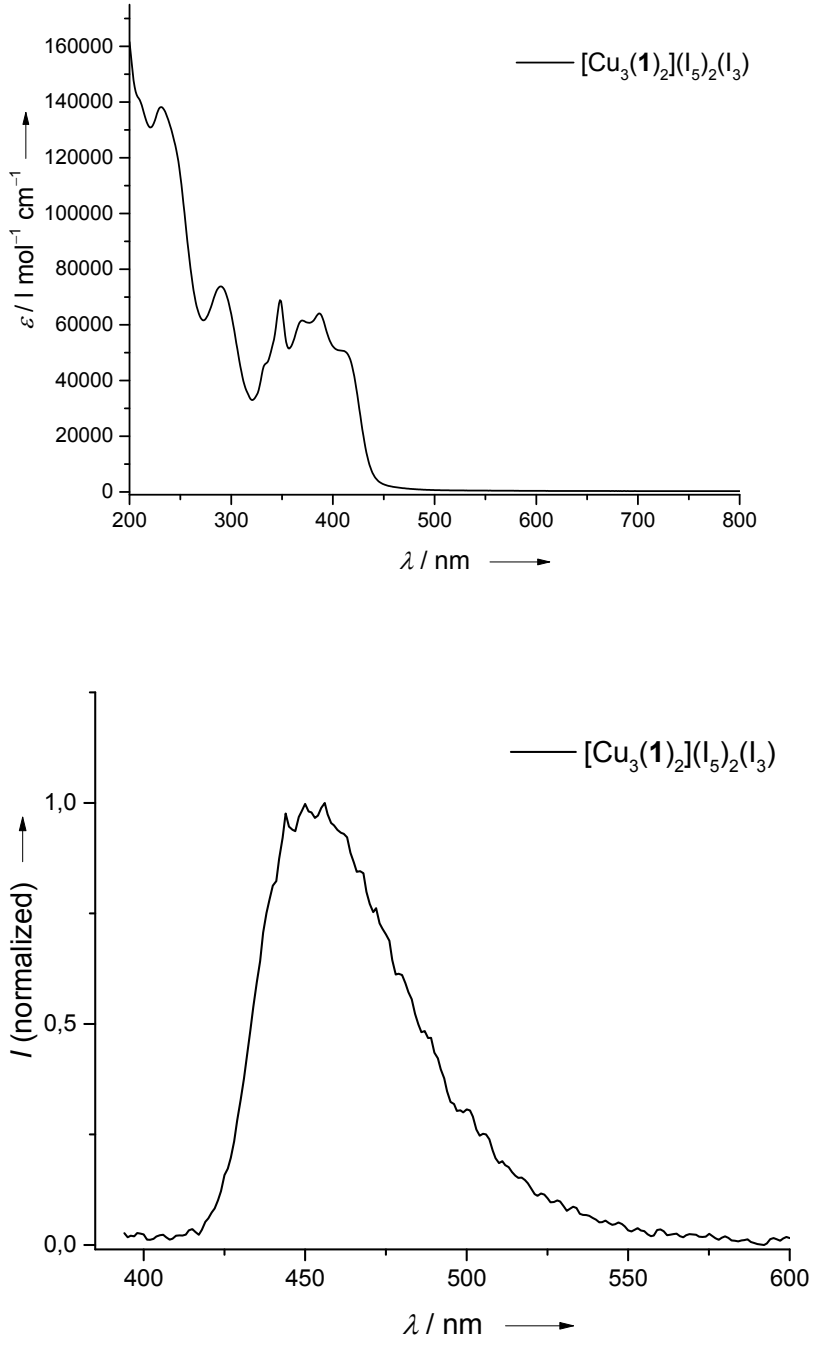

Fig. S21 Top: UV/Vis spectra of $[Cu_3(\mathbf{1})_3](I_5)_2(I_3)$ in CH_3CN ($c = 1.1 \cdot 10^{-5}$ mol l^{-1}). Bottom: Normalized emission spectra of $[Cu_3(\mathbf{1})_3](I_5)_2(I_3)$ in CH_3CN ($c = 1.1 \cdot 10^{-5}$ mol l^{-1}).

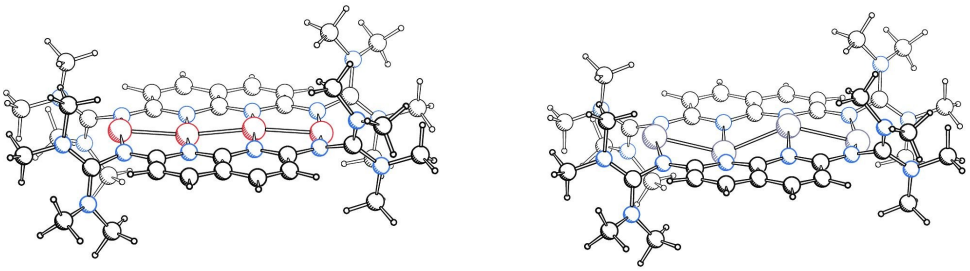

a) b)

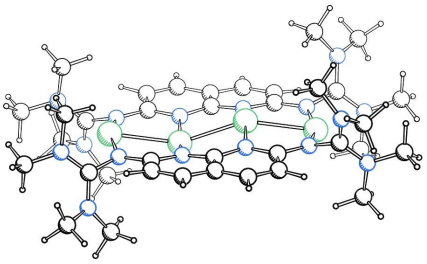

c)

Fig. S22 Calculated minimum structures of a) $[Cu_4(\mathbf{1})_2]^{4+}$, b) $[Ag_4(\mathbf{1})_2]^{4+}$ and c) $[Au_4(\mathbf{1})_2]^{4+}$ (B3LYP/SV(P)).

Quantum chemical calculations

TD-DFT calculations were performed for $[Ag_4(\mathbf{1})_2]^{4+}$ and $[Au_4(\mathbf{1})_2]^{4+}$ to investigate, if the type of the metal atoms of the tetranuclear complex has influence on the electronic excitations. In particular, we were interested, if the exchange of the metal leads to a change of the nature of the low-lying transitions. The spectra are shown in Fig. S23. For $[Ag_4(\mathbf{1})_2]^{4+}$, the two strong low-lying transitions are found at 350.5 and 343.4 nm, they are blue-shifted by 10 and 5 nm with respect to the $[Cu_4(\mathbf{1})_2]^{4+}$ positions. These are HOMO-1 → LUMO and HOMO → LUMO+1 transitions, and the orbitals again are combinations of the HOMOs or the LUMOs of the two ligands. The orbitals are shown in Fig. S24. For $[Au_4(\mathbf{1})_2]^{4+}$, there are two strong low-lying transitions at 360.4 nm and 328.5 nm. These are transitions from the HOMO-1 to LUMO+1 and from the HOMO to LUMO+5 orbitals. The former transition again is a ligand centered transition involving essentially combinations of the HOMOs and LUMOs of the two ligands. However, the latter transition is a transition similar to the

transition of $[Cu_4(\mathbf{1})_2]^{4+}$ at 293 nm, involving the Au d orbitals. The orbitals are shown in Fig. S25. Thus for Au complex, the first strong transition involving the d orbitals is found distinctly red-shifted (35 nm) compared to the Cu complex. Interestingly, for the Ag complex there is no corresponding low-lying transition involving the d orbitals with a sizeable intensity.

Table S2 Selected calculated bond distances (in Å) and angles (in °) for $[Cu_4(\mathbf{1})_2]^{4+}$, $[Ag_4(\mathbf{1})_2]^{4+}$ and $[Au_4(\mathbf{1})_2]^{4+}$ (B3LYP/SV(P).

	$[Cu_4(\mathbf{1})_2]^{4+}$	$[Ag_4(\mathbf{1})_2]^{4+}$	$[Au_4(\mathbf{1})_2]^{4+}$
$M_{terminal}\ldots M_{central}$	2.449	2.696	2.684
$M_{central}\ldots M_{central}$	2.426	2.664	2.633
$M_{central}$-N	1.972	2.226	2.156
$M_{terminal}$-N	1.927	2.181	2.151
N=C	1.386	1.380	1.392
M-M-M	170.70	142.39	152.92

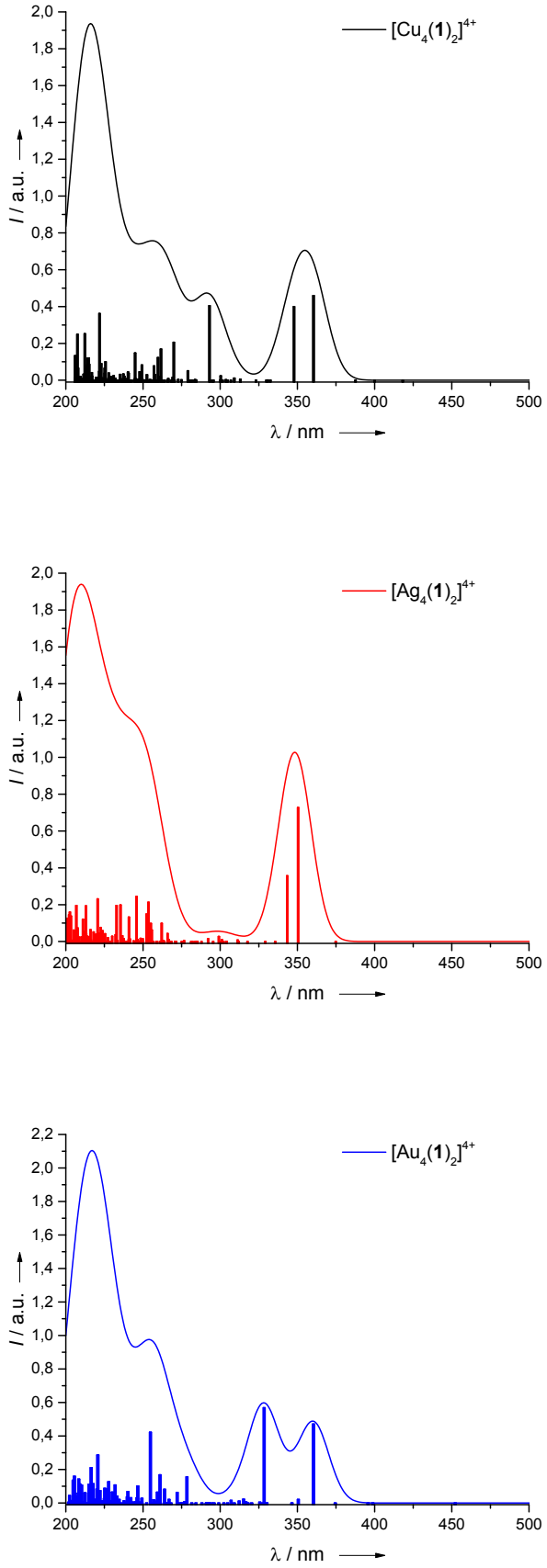

Fig. S23 Theoretical UV/Vis spectrum from TD-DFT calculations (B3LYP/def2-SV(P)) for $[Cu_4(\mathbf{1})_2]^{4+}$ (top), $[Ag_4(\mathbf{1})_2]^{4+}$ (center) and $[Au_4(\mathbf{1})_2]^{4+}$ (bottom). Data was fitted as Gaussian curve with a half-width of 20 nm.

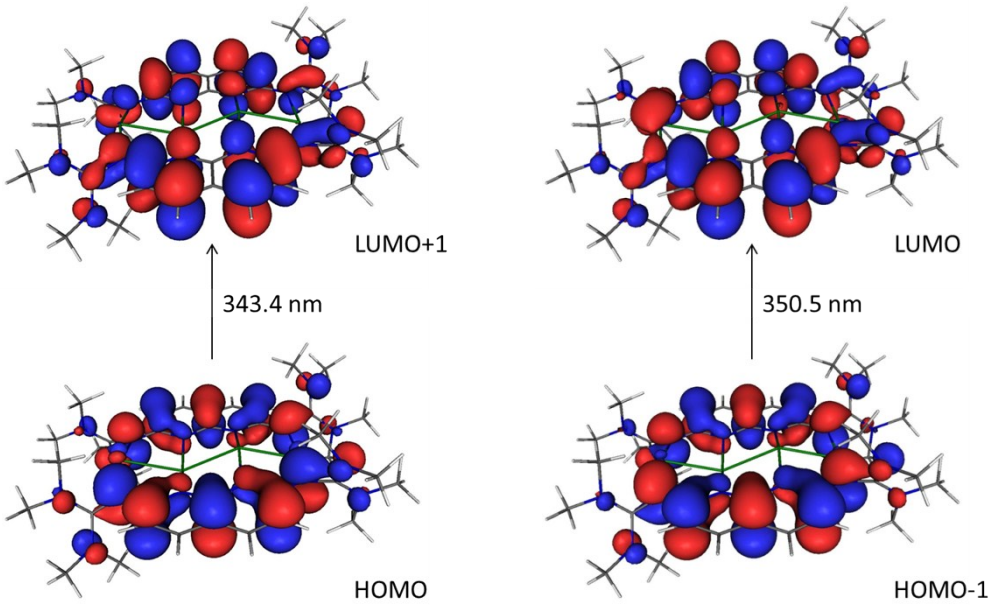

Fig. S24 Visualization of isodensity surfaces of orbitals of $[Ag_4(\mathbf{1})_2]^{4+}$ involved in the electronic transitions.

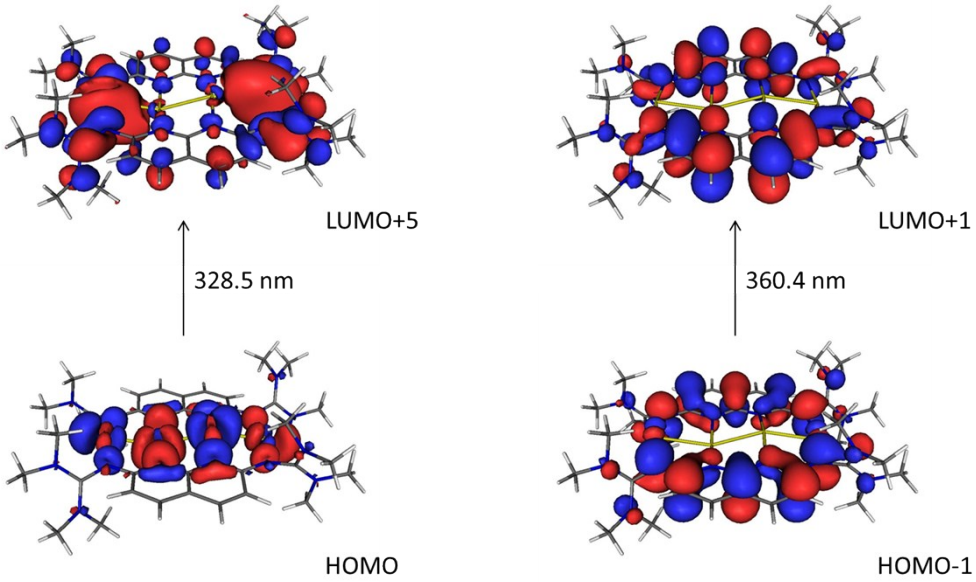

Fig. S25 Visualization of isodensity surfaces of orbitals of $[Au_4(\mathbf{1})_2]^{4+}$ involved in the electronic transitions.